Pressure Drop and Cavitation Optimization of a Relief Valve Featuring Quick Coupling Used in Radar Systems

Yaşar Mutlu[1] · **Aydın Hacı Dönmez[2]** · **Muhammet Ali Karadağ[3]** · **Pınar Göklüberk[3]**

Abstract

This extensive study is carried out to minimize the pressure drop of a relief valve featuring quick-releasing coupling used in radar systems. The 3D two-phase computational fluid dynamic (CFD) study is verified with the experiments, and Taguchi's orthogonal method is implemented for pressure drop optimization. Realizable k–ε turbulence model with enhanced wall treatment and the Schnerr and Sauer cavitation model are enforced within the numerical study. Four angles—the collet angle, the inlet angle, the plug angle, and the outlet angle—are considered at five levels of variation for the orthogonal optimization process. According to the statistical analysis, two more designs are suggested, and one of them resulted in further improved pressure drop performance. Moreover, the cavitation behavior of the proposed design is compared with the base design through water vapor volume fractions. While the water vapor volume fraction of the base design is 0.0045, no vapor formation is observed in the optimized designs at 20 l/min. The results of the proposed design are also validated by the experiments. The outcomes of the study showed that the inlet angle has a significant effect on the pressure drop phenomenon.

List of symbols

G_k	Turbulence kinetic energy generation by velocity gradients
G_b	Turbulence kinetic energy generation by buoyancy
k	Turbulence kinetic energy
M_t	Turbulent Mach number
R_b	Bubble radius
S	Modulus of the mean rate of strain tensor
S_{ij}	Mean strain rate
U	Uncertainty percentage
Y_M	Dilatant dissipation
α	Outlet angle
α_v	Vapor volume fraction
β	Inlet angle
γ	Plug angle
ε	Dissipation rate of turbulence kinetic energy
η	Effectiveness term
μ	Fluid viscosity
μ_t	Turbulent viscosity
ν	Kinematic viscosity
σ	Surface tension of bubble
ρ	Fluid density
ρ_l	Liquid density
ρ_v	Vapor density
σ_k	Turbulent Prandtl number for turbulence kinetic energy
σ_ε	Turbulent Prandtl number for turbulence kinetic energy dissipation rate
ω	Measurement uncertainty
ϕ	Collet angle

✉ Aydın Hacı Dönmez
aydindonmez@halic.edu.tr

Yaşar Mutlu
yasarmutlu@beykent.edu.tr

Muhammet Ali Karadağ
muhammetali.karadag@tst-tamsan.com

Pınar Göklüberk
pinar.celik@tst-tamsan.com

1 Mechanical Engineering Department, Beykent University, Istanbul, Turkey

2 Mechanical Engineering Department, Halic University, Istanbul, Turkey

3 Tamsan Bağlantı Elemanları A.Ş, Izmit, Turkey

Springer

Abbreviations

CFD   Computational fluid dynamics
MSD   Mean squared deviation
RNG   Renormalization group
S/N   Signal-to-noise ratio

1 Introduction

Quick couplings are widely used elements for sustaining rapid connection of lines for any fluid flow. Besides, they can operate as a relief valve when disconnected, if desired. Even though the dynamic behavior of the relief valves has been fairly investigated [1–7], studies related to the quick-releasing couplings are limited.

The quick-releasing couplings are commonly used in the cooling circuits of radar systems. They are preferred due to their ease of connecting and disconnecting properties during maintenance of the serpentine coil in the cooling system. Owing to the fact that the refrigerant passing through the cooling cycle expands during this maintenance period, it is also desired to operate as a relief valve and discharge the required amount of fluid to avoid damage.

Since the connection of the cooling cycle equipment is provided with quick couplings, their pressure drop characteristics come into prominence to minimize local losses and reduce energy consumption.

Gharebaghi et al. [8] performed numerical simulations on a quick coupling used for irrigation to decrease its head loss. Afterward, they carried out a design study by considering various valve components like the dimple head, valve seat, valve seal, and gripping elements. Furthermore, they compared the results of the various k–ε-based turbulence models with the experimental data, showing that the standard k–ε turbulence model results were the best-fitted data with the experiments. According to the results of the parametric study, they proposed a new design and achieved remarkable progress through a head drop. Therefore, they achieved the design of a new quick coupling with a lower head drop using CFD techniques. Finesso and Rundo [9] investigated the flow characteristics of a pressure relief valve and developed a dynamic model that predicts the flow behavior with respect to poppet geometry. The investigation covers the effects of spring setting, poppet cone angle, deflector geometry, and distance from the poppet. A 3D numerical study with a dynamic mesh model is validated with the experiments. Finally, they performed a lumped parameter analysis for the model and claimed that the model was also valid under transient flow conditions. It was found that deflector depth significantly affected the compensation of flow force,

unlike deflector distance and cone angle. So, the dynamic behavior modeling of a quick coupling is accomplished. Kim and Kim [10] optimized a pressure relief valve under cavitation conditions, considering its geometrical features and operating characteristics. Accordingly, they executed transient flow analysis and implemented a genetic algorithm for single- and multi-objective optimization. The three objective functions were utilized to minimize pressure fluctuations, surge damages, and cavitation, respectively. Finally, they presented the flow and cavitation variables using time series as a result of the genetic algorithm study. It is stated that the results of the multi-objective hydraulic structure optimization study provided better cavitation control compared to the single-objective one. Through this study, they utilized artificial intelligence methods for the optimization process. Wu et al. [11] proposed a new design for a conventional hydraulic coupling system with a pressure relief module and achieved lower resistance due to the fluid pressure. Accordingly, they mentioned that the new design can compensate for higher instantaneous pressure values with a lower opening force. Also, they have slightly enhanced the pressure drop value of the coupling system despite its relatively complicated structure. The design procedure is based on 3D numerical studies and a dynamic mesh approach. As a result, better efficiency in hydraulic power transfer is sustained with effortless mounting. Accordingly, they enforced dynamic mesh modeling to procure time-dependent characteristics of the system. Selvam and Logonatham [12] carried out the structural design of a quick coupling and derived the relations for its pressure drop. However, they must still conduct a study to improve pressure drop performance. It is mentioned that a 20% performance enhancement is achieved with the new design. Qin et al. [13] executed a numerical study on relief valves featuring quick-releasing couplings and focused on their structural analysis rather than investigating the flow behavior. According to the fluid–structure interaction-based approach, they compared the deformation, stress, strain, and safety factor values of two different designs.

The studies on relief valves are focused on numerical simulations, either to model their dynamic behavior or to propose a new design for better performance. Scuro et al. [14] performed numerical simulations of a safety relief valve under varying inlet pressure and opening position conditions. They presented the flow variables like pressure, velocity, and discharge coefficient of the valve, considering the compressibility effects. Ultimately, they reported that the valve met the required safety requirements. Accordingly, the effect of inlet pressure on the valve's operation is investigated numerically. Song et al. [15] conducted dynamic modeling of a safety relief valve and carried out transient CFD simulations with the moving grid technique to understand the valve behavior under opening and closing conditions. Furthermore, they integrated a pressure vessel at the inlet instead

of defining a constant inlet pressure boundary condition for a relatively realistic simulation. Also, they presented the valve lift and disk forces throughout the valve operation period. They depicted that their proposed model helps understand the valve's characteristics even if mounted to the line. Thus, the dynamic behavior of the relief valves is studied with dynamic mesh modeling. He et al. [16] investigated the cavitating flow in a relief valve, which operates with oil under varying temperatures, both numerically and experimentally. It is stated that the flow rate is indirectly proportional to the temperature because an increase in temperature results in a decline in the oil viscosity. The Schnerr–Sauer cavitation model is enforced within the numerical study, and the effect of temperature on thermo-physical properties and cavitation intensity is discussed. It is stated that a positive correlation of temperature with velocity and cavitation intensity is secured. Consequently, this study investigates the effect of temperature on the cavitation phenomenon in relief valves. Wu et al. [17] studied a pilot-operated relief valve and realized structural optimization for noise degradation. The simulations are performed with standard-, RNG-, and realizable k–ε turbulence models together with the Zwart–Gerber–Belamri cavitation model, and vapor volume fractions and total vapor amounts are presented to understand the cavitation phenomenon better. Near-wall treatment is performed within the study, and the effects of various geometrical parameters like annular groove structure, outlet piston position, and spool cone angle are examined. The valve port significantly affects the cavitation and is pretty reduced with the proposed design. In this way, CFD methods are executed to reduce the noise of a relief valve. Zhang et al. [18] accomplished a design study of a safety relief valve with the help of a CFD technique based on the response surface method and validated the results with the experiments. The geometrical properties were used as inputs for the response surface method. As a result, they proposed a model that depicts the relationship between blowdown and valve geometry with less than 1% relative error. Furthermore, they could decrease the valve's blowdown to 5.5% from 18.13%. As a result, a regression-based optimization method is enforced to estimate the blowdown characteristics of a relief valve. Desai et al. [19] put through a finite element analysis of a relief valve and investigated its structural strength rather than the fluid flow. Consequently, they proposed a new design for better reliability under higher temperature and pressure applications.

In this paper, pressure drop optimization of a relief valve featuring quick coupling is conducted. For this purpose, a 3D two-phase computational fluid dynamic (CFD) study of the quick coupling is handled. After validating the numerical results with the experiments, an orthogonal table is designed considering four variables: the collet angle, the inlet angle, the plug angle, and the outlet angle for Taguchi optimization. Thereafter, an analysis of variance study is performed to determine the effect of mentioned parameters on the objective function. The results of the statistical analysis study showed that the inlet angle has a crucial impact on the pressure drop. Furthermore, the cavitation characteristics of the valves are presented to provide a better understanding of the pressure drop phenomenon. As a result, a significant enhancement in pressure drop was achieved with the optimization study. This study is novel because no studies exist on pressure drop optimization and cavitation behavior investigation of relief valves featuring quick couplings. Furthermore, in addition to the pressure drop enhancement, the cavitation phenomenon in quick couplings is deeply investigated with two-phase flow simulations. According to the results of the numerical study, a new design is proposed, and the performance characteristics of the new design are also verified through experiments. Furthermore, cavitation characteristics of the base and optimized designs are compared through water vapor volume fractions, which are procured through a two-phase CFD investigation.

2 Numerical Method and Validation

The study initiates with a numerical simulation of the quick-releasing coupling. For this purpose, 3D CFD calculations with a finite volume method approach are carried out to investigate the valve characteristics for varying mass flow rates. Conservation equations are discretized using second-order finite differences. The pressure drop of the valve is calculated using numerical data obtained from CFD simulations. It is evident that the results of the numerical simulations agree with the experimental data. After validation, various numerical simulations are performed at the nominal flow rate according to the orthogonal table obtained using the Taguchi method. Finally, a new valve design is proposed that minimizes the pressure drop after a statistical analysis. Furthermore, two-phase CFD simulations are carried out to monitor the water vapor volume fractions of the base and the proposed design.

2.1 Generation and Independency of Mesh

Unstructured mesh elements are commonly used in skewed flow domains [8, 9, 11, 14, 16, 17, 20]. Accordingly, tetrahedral grid elements are adopted within the computational domain. Since vaporization is possible during fluid flow, capturing relatively high gradients is beneficial along the coupling walls. Accordingly, the enhanced wall treatment approach is implemented. The computational domain and the details of the mesh are shown in Fig. 1.

The second step of the grid generation study comprises determining the appropriate mesh size and grid refinement. It is obvious that more accurate results would be achieved with a finer grid size; however, this will result in a higher

Fig. 1 a Computational domain of the quick coupling, **b** mesh generation on the quick coupling, and **c** grid details on the sharp-edged upstream
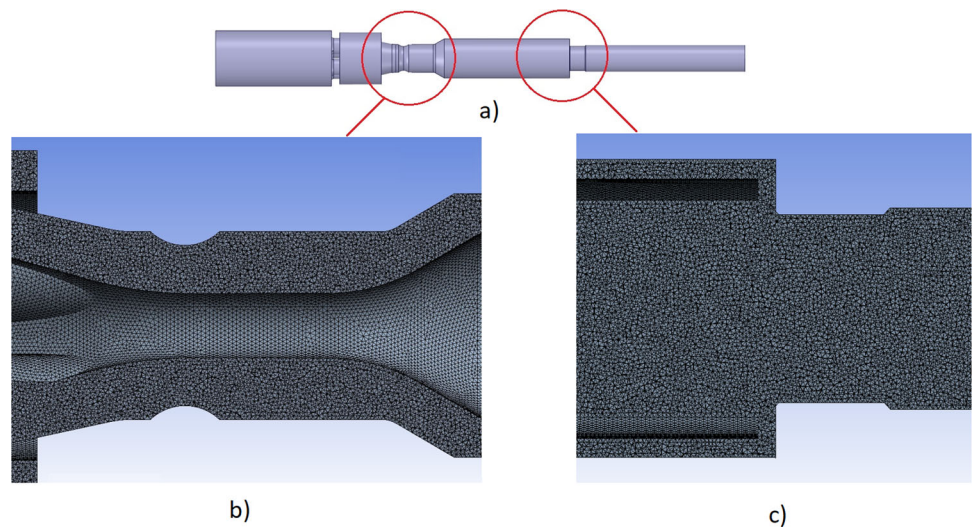

Table 1 Grid independence study

Grid scheme	Element size [mm]	Total number of elements	Pressure drop [Pa]	Variation [%]
Coarse	0.150	12,2 Million	22,643	2.7%
Medium	0.125	21,3 Million	23,280	–
Fine	0.100	43,6 Million	23,343	0.27%

CPU capacity and computational time requirement. Accordingly, a fine grid with a reasonable numerical error will be determined. Due to these reasons, a grid independence study with coarse, medium, and fine grid schemes is implemented in the computation domain within the study. Numerical simulations are performed under the same conditions, and the output of the objective function, which is the pressure drop value of the quick coupling at 6 l/min flow rate, is compared. The results of the grid independence study are tabulated in Table 1.

It is depicted that there is a 2.7% variation in the pressure drop value of the valve when the medium mesh scheme with 21.3 million elements is switched to the coarse mesh scheme with 12.2 million elements. Since this variation is remarkable, a new computational study was performed with a finer grid of 43.6 million elements. In this case, even though the total number of elements exceeds its double, only 0.27% variation in head drop is observed. Therefore, grid independence in the computational domain is assumed to be achieved with the medium mesh scheme. All in all, the numerical simulations are accomplished with the medium-sized mesh scheme.

2.2 Modeling of Turbulence and Cavitation

Even though the standard k–ε turbulence model is robust and gives reasonably accurate results for a wide range of flows, it is claimed that the realizable k–ε turbulence model provides better prediction of wall-bounded flows like channel flows [21]. Furthermore, it performs well for averaging flow fields [22]. The realizable k-epsilon turbulence model with enhanced wall treatment for the ε equation is enforced within the study. Solving the viscous sublayer is helpful, unlike executing a semi-empirical approximation with wall functions. The transport equations for the realizable k–ε turbulence model are introduced below [23].

$$\frac{\partial}{\partial t}(\rho k) + \frac{\partial}{\partial x_j}(\rho k u_j) = \frac{\partial}{\partial x_j}\left[(\mu + \frac{\mu_t}{\sigma_k})\frac{\partial k}{\partial x_j}\right] + G_k + G_b + \rho\varepsilon - Y_M + S_k \tag{1}$$

$$\frac{\partial}{\partial t}(\rho\varepsilon) + \frac{\partial}{\partial x_j}(\rho\varepsilon u_j) = \frac{\partial}{\partial x_j}\left[(\mu + \frac{\mu_t}{\sigma_\varepsilon})\frac{\partial \varepsilon}{\partial x_j}\right] + \rho C_1 S\varepsilon - \rho C_2 \frac{\varepsilon^2}{k + \sqrt{\nu\varepsilon}} + C_{1\varepsilon}\frac{\varepsilon}{k}C_{3\varepsilon}G_b + S_\varepsilon \tag{2}$$

Here, k and ε describe turbulence kinetic energy and the modified version of its dissipation rate, respectively. The turbulence dissipation rate equation is modified considering the fluctuation of the vorticity term in Realizable k-ε turbulence model. Furthermore, the details and definitions of the model constants are shown below:

$$C_1 = \max\left[0.43, \frac{\eta}{\eta + 5}\right] \tag{3}$$

$$\eta = S \frac{k}{\varepsilon} \tag{4}$$

$$S = \sqrt{2 S_{ij} S_{ij}} \tag{5}$$

G_k and G_b are mean velocity gradient-caused and buoyancy-caused turbulence kinetic energy terms, respectively. Y_M is dilatant dissipation and is defined by means of turbulent Mach number (M_t) as:

$$Y_M = 2 \rho \varepsilon M_t^2 \tag{6}$$

S_k and S_ε are source terms. σ_k and σ_ε are turbulent Prandtl numbers for k and ε and equal to 1 and 1.2, individually. $C_{1\varepsilon}$ and C_2 are model constants equal to 1.44 and 1.9, separately.

Mesh refinement is performed, and fine grids are adopted within the computational domain to satisfy the near-wall treatment requirements. One of the primary purposes of the study is to compare the cavitation behavior of the proposed quick coupling with the base design, so cavitation modeling is also provided during the numerical study. Hence, the Schnerr and Sauer cavitation model [24] is implemented based on the Rayleigh–Plesset equation [25]. The generalized Rayleigh—Plesset equation is introduced as follows:

$$R_b \frac{d^2 R_b}{dt^2} + \frac{3}{2} \left(\frac{d R_b}{dt} \right)^2 = \left(\frac{P_b - P}{\rho_l} \right) - \frac{4 v_l}{R_b} \frac{d R_b}{dt} - \frac{2\sigma}{\rho_l R_b} \tag{7}$$

R_b represents the cavitation bubble radius. P_b and P are the pressures of the bubble surface and the far field, respectively. ρ_1 and v_1 depict the liquid's density and kinematic viscosity separately. σ defines the liquid surface tension coefficient. The governing equation of the Schnerr and Sauer cavitation model is introduced below [24]:

$$\frac{\partial}{\partial t} (\alpha_v \rho_v) + \nabla \cdot \left(\alpha_v \rho_v \vec{V} \right) = \frac{\rho_v \rho_l}{\rho} \frac{d\alpha_v}{dt} \tag{8}$$

The mass transfer rate, R, is a source term used to model the phase change.

$$R = \frac{\rho_v \rho_l}{\rho} \alpha_v (1 - \alpha_v) \frac{3}{R_b} \sqrt{\frac{2}{3} \frac{(P_v - P)}{\rho_l}} \tag{9}$$

Additionally, the cavitation bubble radius, R_b, is described with the following equation:

$$R_b = \left(\frac{\alpha_v}{1 - \alpha_v} \frac{3}{4\pi} \frac{1}{n} \right)^{1/3} \tag{10}$$

The variable α in the mass transfer rate and cavitation bubble radius equations indicates the vapor volume fraction
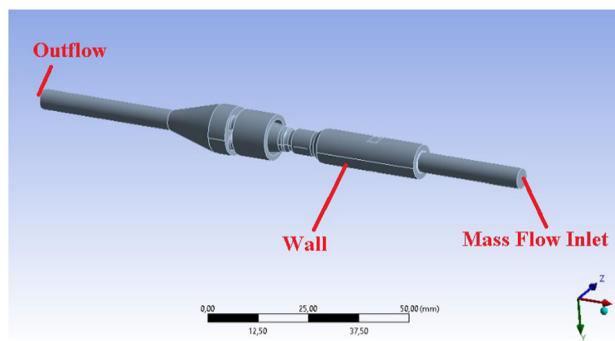

Fig. 2 Boundary conditions

and is characterized as a function of the number of cavitation bubbles and volume ratio.

$$\alpha_v = \frac{n_b \frac{4}{3} \pi R_b^3}{1 + n_b \frac{4}{3} \pi R_b^3} \tag{11}$$

2.3 Boundary Conditions

Mass flow inlet and outflow boundary conditions are adopted upstream and downstream of the flow. With the alteration of the inlet mass flow rate, varying pressure drops are obtained to secure the pressure drop characteristics of the valves. On the other hand, since no flow data are available downstream, an outflow boundary condition is applied at the outlet of the computational domain. The boundary conditions enforced are demonstrated in Fig. 2. The mass flow rate is investigated within the range of 0.067–0.333 kg/s, corresponding to a 4 to 20 l/min volume flow rate.

2.4 Experimental Validation

The pressure drop testing equipment, which consists of two pressure transmitters located upstream and downstream of the tested component, a flowmeter, a ball valve, a centrifugal pump, and a water tank, is used to obtain the pressure drop characteristic of the quick coupling. The circulation of the water is achieved using a centrifugal pump. Flow rate variation is managed with the ball valve, and its values are measured with the flowmeter. The location of the manometers is specified according to the ISO 18869:2017 standards, which specify the testing methods for quick couplings. The illustration of the experimental setup and one of the pressure drop measurements are depicted in Fig. 3.

Even though the required flow rate is 6 l/min in the mentioned radar system operation's cooling cycle, the quick-releasing coupling can operate at higher flow rates. Therefore, the experimental validation of the base study is performed at 4 to 20 l/min in the flow rate range. The measuring
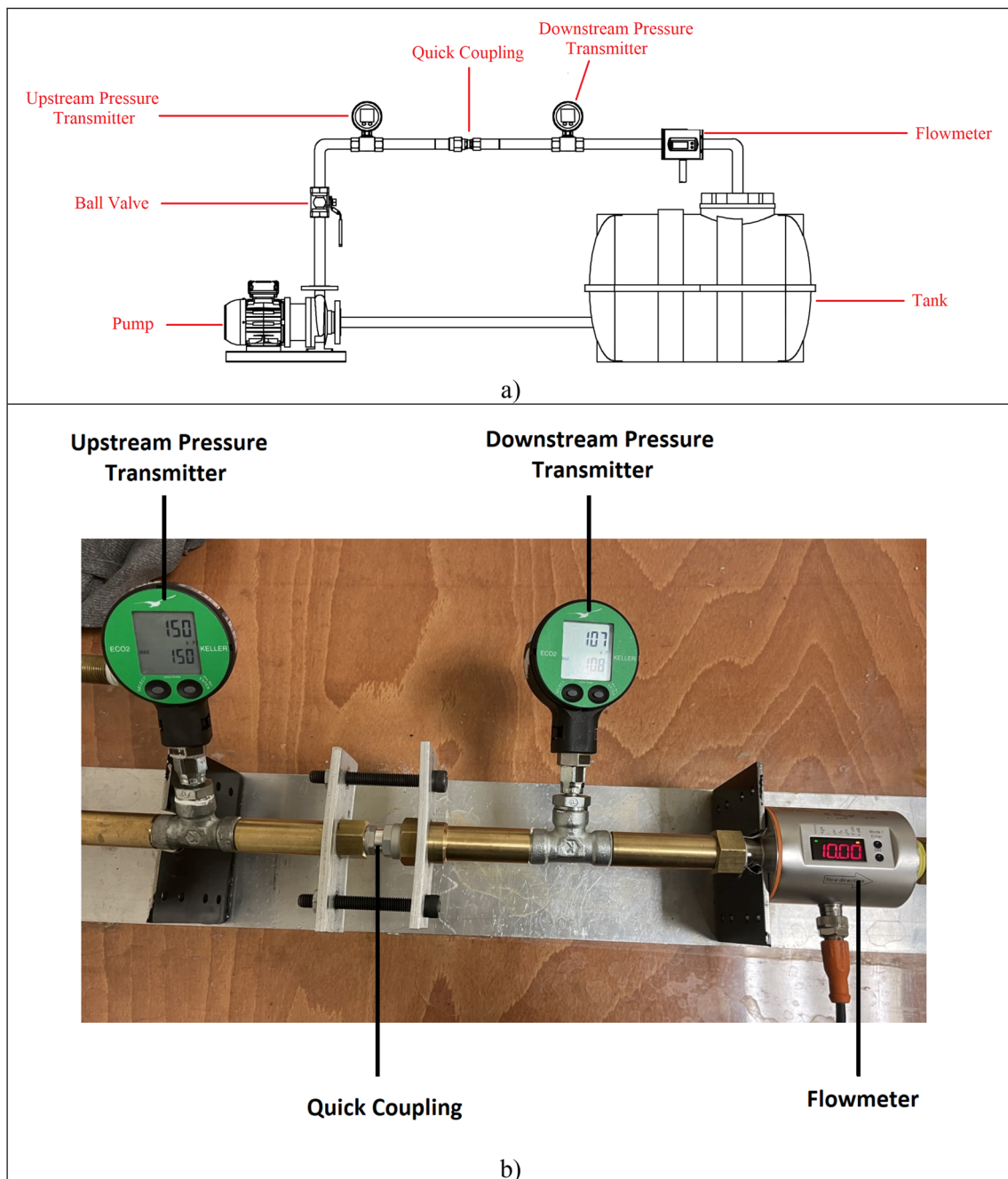
Fig. 3 **a** The scheme of the experimental setup and **b** pressure drop measurements

range of the manometers is -1 to 30 bars, and the maximum measurement error is 0.5% of the measured value at 0 to 50 °C in the operating temperature spectrum. The measurement range for the flowmeter is 0.1 to 25 l/min within the -10 and 70 °C temperature ranges. Its maximum allowable pressure range is 17.7 bars.

For the base design, the numerical pressure drop characteristics are validated with the experiments, and the results are depicted in Fig. 4.

3 Taguchi Optimization

It is possible to determine the best-fitted design of the quick coupling with the highest signal-to-noise ratios (S/N's) of each parameter using the Taguchi method. S/N is defined as the ratio of the signal power to the noise power and refers to the input-to-output relation [26]. Furthermore, the Taguchi method provides fast and robust statistical quality control
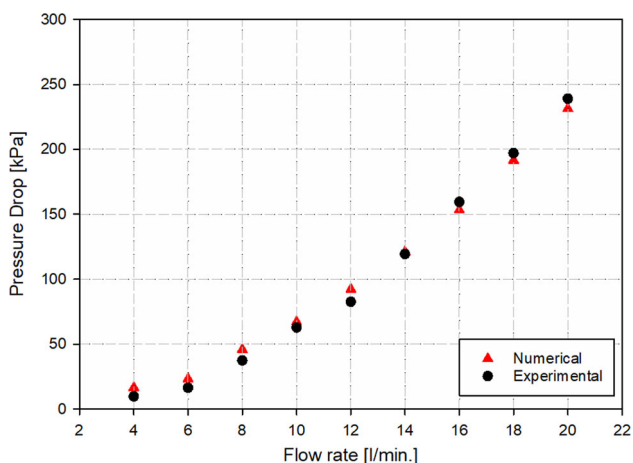
Fig. 4 Validation of the base design

[27]. Parameter selection, the design of experiments concerning the determined parameters and their variations, and variance analysis with the data obtained from the design of the experiment study comprise the different stages of the Taguchi optimization study.

3.1 Selection of Parameters

It is apparent that the flow passes through a narrow and sharp-edged channel inside the quick coupling. Accordingly, four angles have been considered that may have a significant influence on the pressure drop of the valve: the collet angle (Φ), the inlet angle (β), the plug angle (γ), and the outlet angle (α). Although the inlet and collet angles may have the same values for design and manufacturing simplicity as do the outlet and plug angles, they may have different angle values compared individually to each other, either. The layout of the mentioned angles on the quick coupling is presented in Figure 5.

3.2 Design of Experiment and Orthogonal Arrays

The most important advantages of the Taguchi method are its robustness and ease of implementation due to the remarkable decrease in the number of experiments. In this respect, five-level variations of the four factors are considered. Accordingly, the number of experiments is reduced to 25 from $5^4 = 625$ using the L25 orthogonal array. The collet angle, the inlet angle, the plug angle, and the outlet angle values of the base design were 12°, 15°, 30°, and 30°, respectively. Therefore, the collet angle and the inlet angle values are investigated considering 1.5° level steps within the range of 9–15° and 12–18°, respectively. In a similar manner, both the plug angle and the outlet angle are studied with 3°-level steps from 24° to 36°. The L25 orthogonal table with four

parameters and five levels is presented in Table 2. The numbers from 1 to 5 represent each parameter's first to fifth levels in ascending order.

After obtaining the results of the L25 orthogonal array, a statistical analysis will be executed to determine every single angle value that will result in the minimum pressure drop for the quick-releasing coupling.

3.3 Statistical Analysis

A variance analysis study is enforced with the results of the orthogonal table to develop the best design. Taguchi optimization is based on the signal-to-noise ratio, which is the ratio of the desirable value to the undesirable one of the objective functions [28]. S/N is a logarithmic function that calculates the deviation from the objective function and is defined as [29]:

$$\frac{S}{N} = -10 \log(MSD) \tag{12}$$

$$MSD = \frac{y_1^2 + y_2^2 + ... + y_n^2}{n} \tag{13}$$

Three types of S/N exist according to the problem's physics: smaller is better, larger is better, and nominal is better. Since the current study aims to minimize the pressure drop of the valve, the smaller is better model is selected. After that, variance analysis will provide the importance of the parameters.

4 Results and Discussion

Concerning its four basic angles with five levels of variation each, the current study comprises the pressure drop minimization of a quick-releasing coupling. Subsequently, a statistical analysis study is conducted to measure the effect of the collet angle, the inlet angle, the plug angle, and the outlet angle on pressure drop. In addition to the L25 orthogonal table, two more designs are suggested according to the results of the variance analysis. Accordingly, a significant enhancement in the pressure drop characteristic of the quick coupling is achieved compared to the base design. Furthermore, with water vapor fractions acquired with two-phase CFD simulations, the cavitation behavior of the base design is compared with the proposed one. The numerical results of the proposed design are also verified with the experiments.

4.1 Results of the Orthogonal Design and Analysis of Variance

It is stated that 25 different designs are performed considering five-level variations of four factors predicated on the
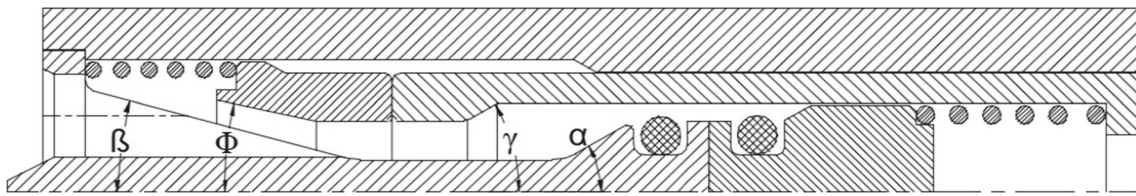
Fig. 5 The arrangement of the parameters on quick coupling geometry

Table 2 L25 orthogonal table

Number of experiments	P1	P2	P3	P4
1	1	1	1	1
2	1	2	2	2
3	1	3	3	3
4	1	4	4	4
5	1	5	5	5
6	2	1	2	3
7	2	2	3	4
8	2	3	4	5
9	2	4	5	1
10	2	5	1	2
11	3	1	3	5
12	3	2	4	1
13	3	3	5	2
14	3	4	1	3
15	3	5	2	4
16	4	1	4	2
17	4	2	5	3
18	4	3	1	4
19	4	4	2	5
20	4	5	3	1
21	5	1	5	4
22	5	2	1	5
23	5	3	2	1
24	5	4	3	2
25	5	5	4	3

L25 orthogonal table. Accordingly, 3D two-phase numerical simulations are performed, and pressure drop values for each design are obtained. Table 3 presents the results of the CFD study.

Table 3 indicates that design 18 resulted in the lowest pressure drop among the 25 designs, with 23,041 Pa. Also, it is seen that the pressure drop value can reach up to 161,280 Pa among 25 designs in the L25 orthogonal table. The optimization study will proceed with the variance analysis study to designate the values of the four factors for the minimum pressure drop.

Signal-to-noise ratios will determine the best value for each of the four factors within the specified levels to achieve the minimum pressure drop for quick coupling. For this purpose, a "smaller is better" type of S/N approach is implemented. The results of the statistical analysis are presented in Fig. 6.

The mean of the signal-to-noise ratio's graph presents the highest S/Ns of each parameter among all levels. Figure 6 shows that the S/N at the inlet angle is significant, and at 15°, the highest signal-to-noise ratio is achieved. On the other hand, the S/N's in the collet angle, the plug angle, and the outlet angle are very close to each other within all levels. Accordingly, focusing on the numerical values of the S/N's is beneficial. Table 4 depicts the numerical values of the signal-to-noise ratios for each level of the parameters.

Table 3 Parameters and results of the objective function for rated flow rate

Number of designs	ϕ (°)	β (°)	γ (°)	α (°)	dP (Pa)
1	9	12	24	24	161,280
2	9	13,5	27	27	160,445
3	9	15	30	30	23,029
4	9	16,5	33	33	23,056
5	9	18	36	36	23,732
6	10,5	12	27	30	161,142
7	10,5	13,5	30	33	160,001
8	10,5	15	33	36	23,365
9	10,5	16,5	36	24	24,775
10	10,5	18	24	27	23,481
11	12	12	30	36	161,185
12	12	13,5	33	24	160,700
13	12	15	36	27	23,766
14	12	16,5	24	30	23,359
15	12	18	27	33	23,633
16	13,5	12	33	27	160,525
17	13,5	13,5	36	30	160,840
18	13,5	15	24	33	23,041
19	13,5	16,5	27	36	23,564
20	13,5	18	30	24	23,954
21	15	12	36	33	160,756
22	15	13,5	24	36	161,227
23	15	15	27	24	23,562
24	15	16,5	30	27	23,599
25	15	18	33	30	23,735

Table 4 shows that the highest signal-to-noise ratios are observed at the first level of the collet angle, the third level of the inlet angle, and the fourth level of the outlet angle, respectively. However, the highest S/N for the plug angle is obtained at its first and fourth levels. Therefore, two more designs are prepared for CFD studies in addition to the L25 orthogonal table. Design 26 is comprises the first level of the collet angle, the third level of the inlet angle, the first level of the plug angle, and the fourth level of the outlet angle, respectively. Similarly, design 27 is built with the first level of the collet angle, the third level of the inlet angle, the fourth level of the plug angle, and the fourth level of the outlet angle, respectively. In other words, design 27 differs from its plug angle value only from Dedign 26. After that, designs 26 and 27 are subjected to the same numerical procedure implemented for the designs in the L25 orthogonal table, and their drop values are calculated. Table 5 provides a comparative evaluation of the new designs proposed after the statistical analysis, and the best design in the L25 orthogonal table and the base design.

The table above presents the values of the parameters that constitute the best design in the L25 orthogonal table, two proposed designs after an analysis of variance study, and the base design. It is depicted that there is a remarkable decrease in the pressure drop with the design acquired in the Taguchi optimization study (Design 18). In addition, further enhancement in pressure drop is noticed with one of the designs (Design 27) suggested from the statistical analysis study with the data from the L25 orthogonal table. Consequently, design 27 was recommended as the best design after the Taguchi optimization study, and it was manufactured to validate the numerical results.

4.2 Cavitation Behavior Comparison of the Designs

In this section, the cavitation behaviors of the base and optimized designs are examined for a better understanding of the pressure drop phenomenon and to visualize the enhancement in the pressure drop of the optimized geometry. Even though the CFD-based design optimization of quick couplings and relief valves exists, their two-phase flow behavior has yet to
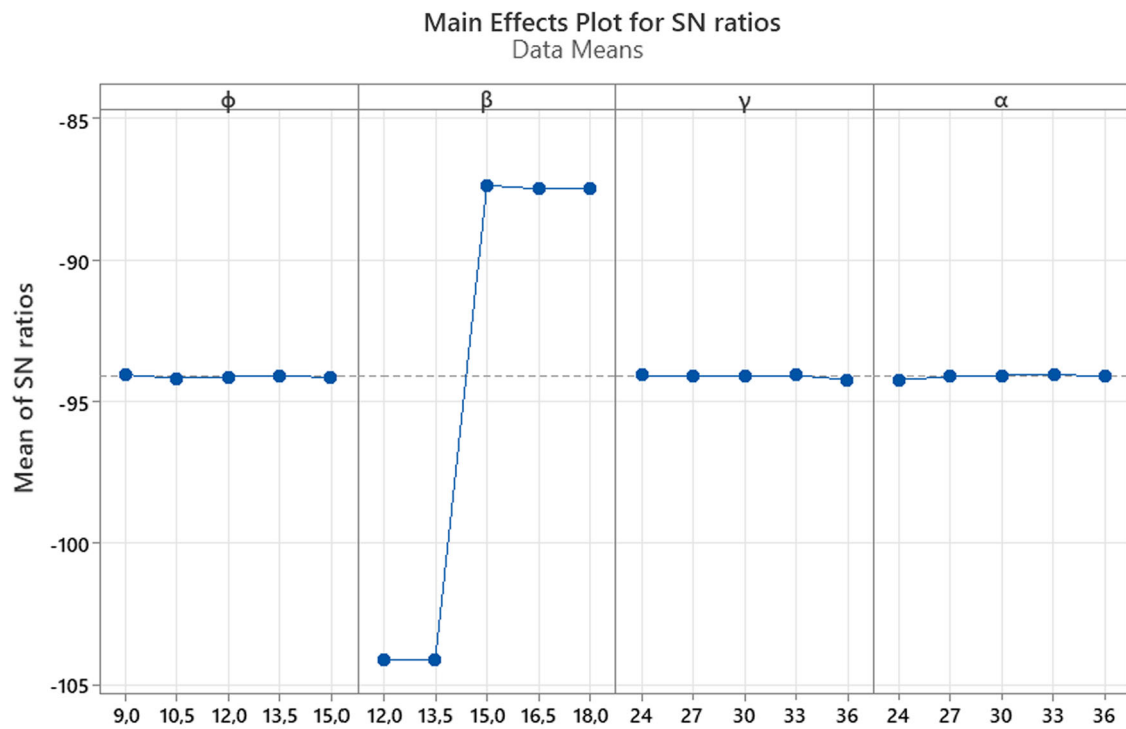
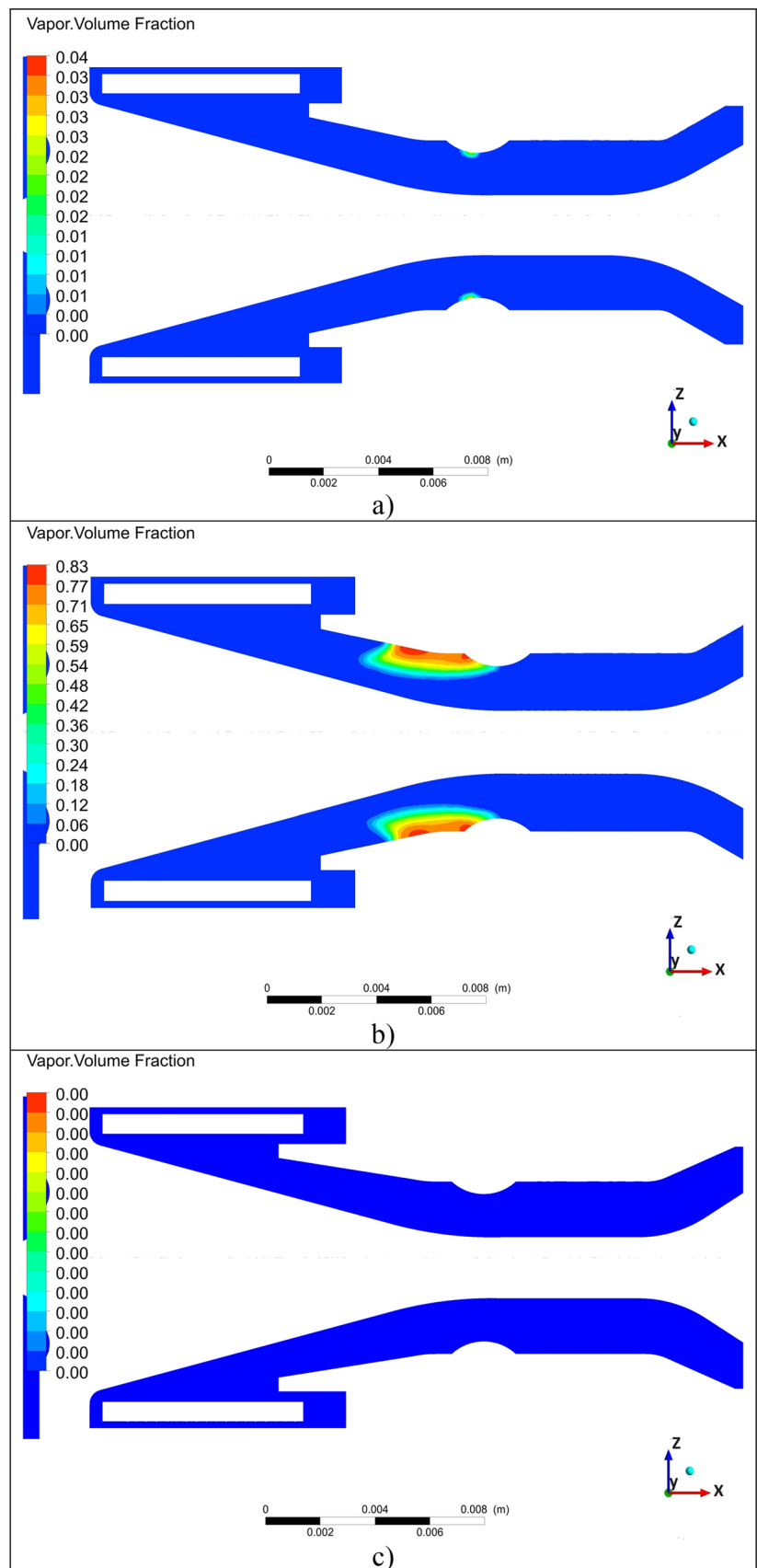Fig. 6 Results of the signal-to-noise ratios for smaller are better approach

Table 4 Values of the signal-to-noise ratios for parameters

Smaller is better				
Level	ϕ (°)	β (°)	γ (°)	α (°)
1	−94,05	−104,14	−94,07	−94,24
2	−94,18	−104,12	−94,12	−94,12
3	−94,13	−87,37	−94,10	−94,08
4	−94,10	−87,48	−94,07	−94,04
5	−94,14	−87,50	−94,23	−94,12
Delta	0,13	16,77	0,16	0,20
Rank	4	1	3	2

Table 5 Pressure drop of the proposed designs with the base design

	ϕ (°)	β (°)	γ (°)	α (°)	dP (Pa)
Base Design	12	15	30	30	23,280
Design 18	13,5	15	24	33	23,041
Design 26	9	15	33	33	23,043
Design 27	9	15	24	33	22,781

Fig. 7 Water vapor volume fractions for **a** base design at 14 l/min, **b** base design at 20 l/min, and **c** optimized design at 20 l/min

Fig. 8 Validation of the optimized design

Fig. 9 Measurement uncertainty of the base and optimized designs
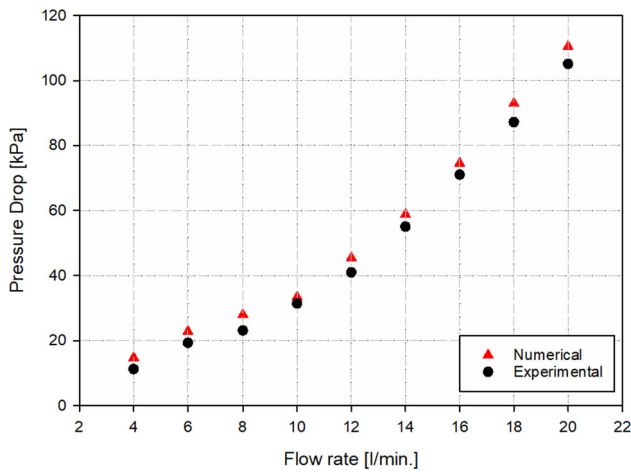
be investigated. In this regard, two-phase CFD simulations are accomplished on the base and optimized geometries for varying flow rate conditions. The results of the present work are depicted through water vapor volume fractions along the radial cross-section of the fluid flow. The results of the two-phase study are presented in Fig. 7.

The water vapor formation at 6 l/min is quite limited, so the results of the two-phase simulations for the mentioned flow rate are not presented in Fig. 7. On the other hand, water vapor development in the flow passage meets the eye at 14 l/min for the base design, and it further accumulates at a flow rate of 20 l/min. However, no water vapor formation is observed even at a flow rate of 20 l/min for the optimized design. This situation also clarifies the results of the pressure drop study. Water vapor volume fractions are 6.5×10^{-7} and 4.5×10^{-3} for the base design at 14 l/min and 20 l/min flow rate conditions, respectively. The pressure drop values at 20 l/min flow rate conditions for the base and optimized designs are 239 and 95 kPa, respectively.

4.3 Validation of the Optimized Design

During the validation of the optimized design, a similar testing procedure is implemented for the optimized quick coupling as in the base design validation study. The experiments are conducted under the same flow rate conditions for a better evaluation. The comparison of the experimental and numerical results for the optimized geometry is introduced in Fig. 8.

4.4 Uncertainty Analysis of the Experimental Studies

Calculating the uncertainty of the experimental studies is an essential issue in estimating their propagation. During experimental studies, the pressure drop of the quick couplings is
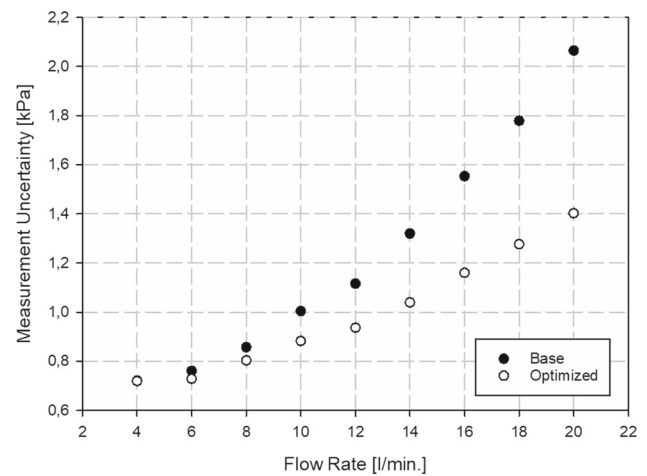
calculated using the inlet and outlet pressures of using two pressure transmitters located upstream and downstream of the flow. Thus, inlet and outlet pressures are the independent variables for the pressure drop. From this aspect, the measurement uncertainty, ω_R, is expressed with the following formulation [30]:

$$\omega_R = \left[\left(\frac{\partial \Delta P}{\partial P_1} \omega_{P_1} \right)^2 + \left(\frac{\partial \Delta P}{\partial P_2} \omega_{P_2} \right)^2 \right]^{1/2} \tag{14}$$

where ω_{P1} and ω_{P2} are the uncertainties of inlet and outlet pressure measurements, respectively. The pressure drop is defined employing inlet and outlet pressures as:

$$\Delta P = P_2 - P_1 \tag{15}$$

On the occasion of using identical manometers at the inlet and outlet, Eq. 14 can be simplified to:

$$\omega_R = \sqrt{P_1^2 + P_2^2} \cdot (\%U) \tag{16}$$

Here, U represents the uncertainty percentage in the pressure measurements. The measurements are executed with manometers with 0.5% uncertainty. The total measurement uncertainties of the base and optimized designs are depicted in Fig. 9 for varying flow rates. The results show that the maximum uncertainty value is around 2 kPa for the base design at the highest flow rate and further less for the optimized one.

5 Conclusions

In this study, pressure drop optimization of a relief valve featuring quick-releasing coupling is carried out in to decrease the power requirement in the cooling cycle of the radar

systems. This study should be considered novel due to the implemented method and the further two-phase numerical investigation of unique equipment. Additionally, the validation of the numerical study is achieved successfully for both base and optimized models. The main findings of the study are as follows:

a. Four main parameters, the collet angle, the inlet angle, the plug angle, and the outlet angle, are specified as the design parameters for the quick coupling, and the inlet angle significantly affects the pressure drop phenomenon.
b. The mesh structure and size influence numerical results, so a grid refinement study with a near-wall treatment is conducted, and the largest deviation in the experimental and numerical results of the pressure drop values is obtained as 4.2%.
c. With the optimized geometry, an enhancement of 6.2%, 55.6%, and 60.2% is achieved in the pressure drop for 6 l/min, 14 l/min, and 20 l/min flow rate conditions, respectively.
d. Two-phase CFD simulations show that up to 4% and 83% water vapor regions were observed locally for the base design at 14 l/min and 20 l/min flow rate conditions, respectively. However, no water vapor region is observed for the optimized design, even at a flow rate of 20 l/min.
e. The total measurement uncertainties are less than 1 kPa for operating conditions. Furthermore, the maximum uncertainties are 2.06 and 1.40 kPa for the base and optimized models, respectively.
f. More precise results could be obtained with decreasing level steps and/or increasing levels. However, this situation will lead to a major increase in the computational time requirement. Further improvement on the pressure drop could be achieved by enforcing machine learning methods.
g. This research would fill the gap in the deficiency of studies related to relief valves featuring quick couplings and provide a basis for future studies.

Data Availability The data will be available upon request.

Declarations

Conflict of interest The author's declare that they have no known competing interests.

References

1. Ray, A.: Dynamic modeling and simulation of a relief valve. Simul. **31**(5), 167–172 (1978)
2. Zung, P.S.; Perng, M.H.: Nonlinear dynamic model of a two-stage pressure relief valve for designers. J. Dyn. Syst.-T. Asme. **124**(1), 62–66 (2002)
3. Maiti, R.; Saha, R.; Watton, J.: The static and dynamic characteristics of a pressure relief valve with a proportional solenoid-controlled pilot stage. P. I. Mech. Eng., Part I J. Syst. **216**(2), 143–156 (2002)
4. Darby, R.: The dynamic response of pressure relief valves in vapor or gas service, part I: Mathematical model. J. Loss. Prevent. Proc. **26**(6), 1262–1268 (2013)
5. Sverbilov, V.; Stadnick, D.; Makaryants, G.: Study on dynamic behavior of a gas pressure relief valve for a big flow rate. Fluid Power Syst. Technol. (2013). https://doi.org/10.1115/FPMC2013-4479
6. Erdődi, I.; Hős, C.: Prediction of quarter-wave instability in direct spring operated pressure relief valves with upstream piping by means of CFD and reduced order modelling. J. Fluid. Struct. **73**, 37–52 (2017)
7. Zhang, Z.; Jia, L.; Yang, L.: Numerical simulation study on the opening process of the atmospheric relief valve. Nucl. Eng. Des. **351**, 106–115 (2019)
8. Gharebaghi, P.; Ahmadi, H.; Hemmati, M.; Rezaverdinejad, V.: Optimization of an effective quick coupling valve for pressurized irrigation. Irrig. Drain. **70**(4), 690–704 (2021)
9. Finesso, R.; Rundo, M.: Numerical and experimental investigation on a conical poppet relief valve with flow force compensation. Int. J. Fluid Power **18**(2), 111–122 (2017)
10. Kim, H.; Kim, S.: Optimization of pressure relief valve for pipeline system under transient induced cavitation condition. Urban. Water. J. **16**(10), 718–726 (2019)
11. Wu, Y.T.; Qin, Z.; Eizad, A.; Lyu, S.K.: Design and numerical simulation-based optimization of a novel flat-face coupling system for hydraulic power equipment. Appl. Sci.-Basel. **11**(1), 388 (2021)
12. Selvam, R.; Loganathan, G.B.: Product detail and analysis of hydraulic quick releasing coupling. Mater. Today.-Proc. **22**, 751–755 (2020)
13. Qin, Z.; Tang, X.; Wu, Y.T.; Lyu, S.K.; Park, S.: Design and structural stability investigation of novel flat-face multi-coupling systems for hydraulic power equipment. Int. J. Precis. Eng. Man. **23**(10), 1183–1202 (2022)

14. Scuro, N.L.; Angelo, E.; Angelo, G.; Andrade, D.A.: A CFD analysis of the flow dynamics of a directly-operated safety relief valve. Nucl. Eng. Des. **328**, 321–332 (2018)

15. Song, X.; Cui, L.; Cao, M.; Cao, W.; Park, Y.; Dempster, W.M.: A CFD analysis of the dynamics of a direct-operated safety relief valve mounted on a pressure vessel. Energ. Convers. Manage. **81**, 407–419 (2014)

16. He, J.; Zhang, Y.; Liu, X.; Li, B.; Sun, S.; Peng, J.; Liu, W.: Experiment and simulation study on cavitation flow in pressure relief valve at different hydraulic oil temperatures. Flow Meas. Instrum. **89**, 102289 (2023)

17. Wu, W.; Qiu, B.; Tian, G.; Liao, X.; Wang, T.: CFD-based cavitation research and structure optimization of relief valve for noise reduction. IEEE. Access. **10**, 66356–66373 (2022)

18. Zhang, J.; Yang, L.; Dempster, W.; Yu, X.; Jia, J.; Tu, S.T.: Prediction of blowdown of a pressure relief valve using response surface methodology and CFD techniques. Appl. Therm. Eng. **133**, 713–726 (2018)

19. Desai, S.; Desai, A.; Karande, V.: Design and weight optimization of buffer relief valve using FEA with experimental validation. Mater. Today.-Proc. **27**, 1466–1472 (2020)

20. Asli, H.H.; Nazari, S.: Water age and leakage in reservoirs; some computational aspects and practical hints. LARHYSS J. **48**, 151–167 (2021)

21. Shih, T.H.; Liou, W.W.; Shabbir, A.; Yang, Z.; Zhu, J.: A new k-ϵ eddy viscosity model for high reynolds number turbulent flows. Comput. Fluids. Fluids **24**(3), 227–238 (1995)

22. Zheng, L.; Lu, W.; Wu, L.; Zhou, Q.: A review of integration between BIM and CFD for building outdoor environment simulation. Build. Environ. **228**, 109862 (2023)

23. Ansys Fluent 2022 R2 Theory Guide.: ANSYS Inc., Canonsburg, PA (2022)

24. Schnerr, G. H.; Sauer, J.: Physical and numerical modeling of unsteady cavitation dynamics. In fourth international conference on multiphase flow (Vol. 1) (2001)

25. Brennen, C.E.: Cavitation and Bubble Dynamics. Oxford University Press, New York (1995)

26. Taguchi, G.; Chowdhury, S.; Wu, Y.: Taguchi's Quality Engineering Handbook. John Wiley & Sons Inc, Michigan (2004)

27. Aslan, N.: Multi-objective optimization of some process parameters of a multi-gravity separator for chromite concentration. Sep. Purif. Technol. **64**(2), 237–241 (2008)

28. Do Kim, K.; Kim, S.H.; Kim, H.T.: Applying the Taguchi method to the optimization for the synthesis of TiO_2 nanoparticles by hydrolysis of TEOT in micelles. Colloid. Surface. A. **254**(1–3), 99–105 (2005)

29. Kumar, A.; Sharma, C.: Fine and targeted tuning of a single quadrupole MS hyphenated with gas chromatography using Taguchi method. Microchem. J. **195**, 109491 (2023)

30. Holman, J.P.: Experimental Methods for Engineers. McGraw-Hill, New York (2001)